Pergamon

Int. J. Heat Mass Transfer. Vol. 37, No. 16, pp. 2561–2569, 1994

0017-9310/94 $7.00+0.00

0017-9310(94)E0068-6

The onset of film boiling on small cylinders: local dryout and hydrodynamic critical heat flux mechanisms

S. M. YOU, Y. S. HONG and J. P. O'CONNOR

Department of Mechanical Engineering, University of Texas at Arlington, Arlington, TX 76019-0023, U.S.A.

(*Received* 27 *July* 1993 *and in final form* 31 *January* 1994)

Abstract—Pool boiling experiments are performed to investigate the onset of film boiling mechanisms on small horizontally oriented cylinders ranging in diameter from 11 to 510 μm. Three test liquids are used, FC-72, R-113 and methanol. Photographs indicate the existence of two mechanisms which proceed film boiling, hydrodynamic critical heat flux (CHF) and local dryout. The hydrodynamic CHF mechanism is observed for dimensionless radius (R') values as low as 0.0123. This leads to a modified version of Sun and Lienhard's hydrodynamic CHF correlation for cylindrical geometries which was developed in 1970. The local dryout mechanism is governed by boiling incipience phenomena. A method for predicting the local dryout heat flux for these conditions is presented.

INTRODUCTION

IN 1934, NUKIYAMA [1] conducted a pool boiling experiment by controlling heat flux. He observed a local maximum heat flux, q_{max}, and noted that any additional increase beyond q_{max} would result in a significant increase in surface temperature (T_w). The heat flux value corresponding to this phenomenon is called the "Critical Heat Flux" (CHF) or "Departure from Nucleate Boiling" (DNB). Many investigators have labored to predict the CHF on various geometries and at various conditions. In 1952, Kutateladze [2] developed a correlation predicting the CHF based on a dimensional analysis of available data. In 1959, Zuber [3] developed a prediction of the hydrodynamic CHF on an infinite horizontal flat plate which reduces to the following equation at 1 atm:

$$q_{max_z} = \frac{\pi}{24}\sqrt{(\rho_g)}\, h_{fg}\,[\sigma g(\rho_f - \rho_g)]^{1/4}. \quad (1)$$

Zuber's correlation was referenced by several investigators who accounted for geometry effects.

In 1964, based on cylindrical geometry experimental results, Lienhard and Wong [4] suggested that CHF was strongly dependent upon the radius. In 1966, Lienhard and Watanabe [5] correlated the CHF against pressure and cylindrical heater geometry and successfully applied it to their data. The resulting correlation concluded that the effect of cylinder radius on the CHF for "small" wires is significant, and also that the CHF is strongly dependent on geometry and gravity. In 1970, Sun and Lienhard [6] proposed a hydrodynamic prediction for the CHF of cylinders as a function of a dimensionless radius (R'):

$$\frac{q_{max}}{q_{max_z}} \cong 0.89 + 2.27\,e^{-3.44\sqrt{R'}};\ R' > 0.15 \quad (2)$$

where

$$R' = R\sqrt{[g(\rho_f - \rho_g)/\sigma]}. \quad (3)$$

They observed for R' values greater than 3.47, the dimensionless CHF, equation (2), approaches 0.89. Figure 1, taken from Sun and Lienhard [6] illustrates the dimensionless CHF dependence on R'. The figure includes over 900 data for various test liquids and cylinders. Sun and Lienhard's correlation, equation (2), is represented by the solid line. For values of R' greater than 0.15, the experimental data agree to within ±20% of the prediction. For values of R' less than 0.15, the data begin to deviate from the prediction and the scatter among data increases. The present study is focused to investigate the CHF for values of R' less than 0.15, where wide scatter in the data is observed.

Bakhru and Lienhard [7] conducted a pool boiling investigation with small cylinders immersed in four organic liquids and water. One of the primary conclusions was for R' values less than 0.01, no local maxima or minima existed in the boiling curve, therefore the hydrodynamic instabilities which cause these extremes are absent. Their motion pictures indicated that a region of patchy boiling exists beyond the natural convection region. This was identified as a region of mixed natural convection and film boiling. The hydrodynamic mechanism begins to re-establish itself and a small nucleate boiling region was identifiable as R' increased. They felt that the hydrodynamic mechanisms appeared to be fully recovered at R' values between 0.12 and 0.15.

NOMENCLATURE

g	gravitational acceleration	r_c	cavity mouth radius
h_{fg}	latent heat of vaporization	T	temperature
P_l	liquid pressure	T_w	wall temperature
q_{max}	heat flux at the onset of film boiling (hydrodynamic CHF/local dryout)	T_{sat}	saturation temperature
		ΔT	wall superheat, $T_w - T_{sat}$
q_{max_z}	Zuber's CHF prediction for infinite horizontal flat plates	v	specific volume.
R	cylindrical heater radius	Greek symbols	
R'	dimensionless radius	$\rho_f(\rho_g)$	saturated liquid/vapor density
r_b	embryonic bubble radius	σ	surface tension.

EXPERIMENTAL APPARATUS AND PROCEDURE

Test facility

The pool boiling test facility is shown in Fig. 2. The primary components are a polycarbonate water tank and a submerged test liquid vessel. Three liquids are used to conduct the tests, R-113 (trichlorotrifluoroethane), methanol (99.9%) and FC-72 (Fluorinert). These liquids were selected because the ratio between the surface tension and buoyancy force provides a wide range of R', equation (3), for the wire sizes tested. An aluminum test vessel with observation windows is used for the experiment of R-113. When testing FC-72 and methanol, a glass jar is used as the test vessel. Water temperature is controlled by a 1000 Watt immersion circulator–heater and an immersion cooler. A water-cooled condenser is used to degas and reduce any significant loss of the test liquid. Atmospheric pressure is maintained by venting the test vessel through the condenser. A magnetic stir bar located inside the test vessel is used to expedite the degassing process.

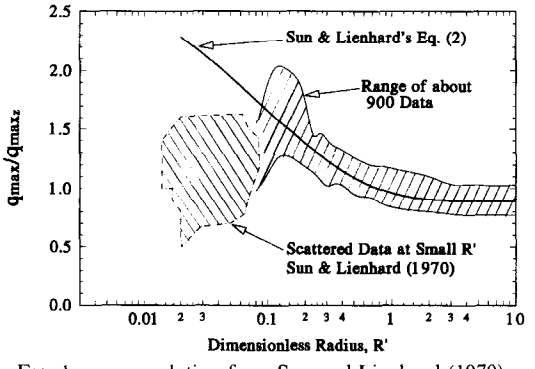

FIG. 1. q_{max} correlation from Sun and Lienhard (1970).

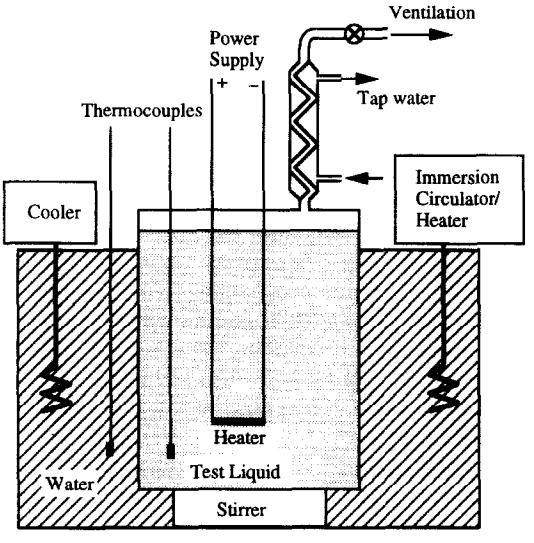

FIG. 2. Experimental apparatus.

Six heaters were tested, three 99.99% pure platinum wires, two nichrome ($Ni_{80}Cr_{20}$) wires, and one nickel wire. The combinations of the wires and test liquids are listed in Table 1. A Scanning Electron Microscope (SEM) was used to photograph and measure wire diameters. The wire heater is mounted tightly by soldering it between two end tips of gauge 10 copper terminals which are mounted in a polycarbonate block. Voltage sensors and a power supply are connected to the heater via the copper terminals. The power supply is connected in series with a standard resistor and the heater. The standard resistor is used to determine the current passing through the wire heater. The resistance is 0.09998 Ω and is accurate to ±0.05%. Direct current is supplied by a power supply to the heating element. This equipment is interfaced via IEEE-488 cables and controlled by a computer. Test and bulk liquid temperature are measured using copper–constantan thermocouples which were calibrated with a precision thermometer.

A unique property of platinum and nickel is a linear temperature–resistance characteristic for a wide range of temperatures. A temperature vs resistance calibration is conducted for each wire heater prior to testing by measuring the resistance of the heater at various temperatures. A set of temperature vs resistance data yield the temperature–resistance slope, dT/dR. The surface temperature of the heater is determined from the calibration curve.

Video imaging equipment was used to record and capture the bubble phenomena associated with the onset of film boiling mechanisms, local dryout and hydrodynamic CHF. The current system (Sony Model CCD-

Table 1. Tested cylindrical heaters and liquids

Test liquid		Heater material	Diameter (μm)	Length (cm)	Dimensionless radius, R'
FC-72	†	Nickel	11	0.5	0.0076
	‡	Platinum	25	1	0.0172
	‡	Platinum	55	2	0.0379
	‡	Platinum	75	2	0.0517
	‡	Nichrome	140	4	0.0965
	‡	Nichrome	510	4	0.3515
R-113	†	Nickel	11	0.5	0.0054
	‡	Platinum	25	1	0.0123
	‡	Platinum	55	2	0.0271
	‡	Platinum	75	4	0.0369
Methanol	†	Nickel	11	0.5	0.0034
	†	Platinum	25	1	0.0078
	†	Platinum	55	2	0.0172
	†	Platinum	75	4	0.0234

†Local dryout conditions.
‡Hydrodynamic CHF conditions.

V801) is capable of shutter speeds up to 1/10 000th of a second and has a fixed speed of 60 frames per second. The camera provides capability to "freeze" the growing and departing bubbles on the wire every 1/30th of a second. Using a focal length of ~30 cm, the resulting magnification factor is approximately 10. Lighting is provided to obtain the highest quality video signal.

Test procedure

The immersion circulator–heater and the magnetic stirrer are turned on and the test liquid is heated to the saturation temperature. Stabilization of liquid temperature is automatically monitored. Once the test liquid reaches its saturation temperature, it is left at this state for 3–4 h to remove the dissolved gases. The magnetic stir bar expedites the degassing process. After degassing, the magnetic stirrer is shut off and data acquisition begins.

Heat flux is increased by controlling the supply voltage. The computer collects 200 data points and calculates heat flux and heater surface temperature over an 18 s time interval. The average surface temperature value of the 51st to 100th data points and the 151st to 200th data points are compared. If the difference is less than 0.2°C, it is assumed that steady-state conditions exist. Under steady-state conditions the mean heat flux and wall superheat values of the last 50 data points are recorded. This completes the acquisition for one data point. If steady-state conditions are not achieved, the process is repeated until the criterion for steady-state is satisfied.

Three different heat flux increments are used. In the natural convection region a large increment of 2 W cm^{-2} is used; after boiling is initiated, 1 W cm^{-2} is used; and when the CHF is approached, a small increment of 0.5 W cm^{-2} is used. For every measurement, the heater surface temperature is compared to its previous averaged value to detect hydrodynamic CHF or local dryout occurrence. If a temperature increase greater than 20°C is detected, the power supply is shut off instantaneously. The heater resistance is measured before and after each run to confirm any occurrence of hysteresis or damage in the heating element. Each case (liquid–heater combination) consists of ten runs. A new wire is mounted for each case. All procedures are computer controlled for consistency.

RESULTS AND DISCUSSION

Table 1 identifies the liquid–heater combinations used in the current study. Two highly-wetting liquids, FC-72 and R-113, and one non-highly-wetting liquid, methanol, along with six wire sizes, lead to 14 test conditions (R' values). All the current data were measured at 1 atm. and at the respective saturation temperature of the test liquid. Using the methods of Kline and McClintock [8], the estimated uncertainties are 6% and 0.4°C for the heat flux and temperature measurements, respectively. The variation in wire diameter is included in the estimated 6%.

This study characterizes the onset of film boiling mechanisms, local dryout and hydrodynamic CHF, of small cylinders for a wide range of R' values ($0.0034 < R' < 0.3515$). The new terminology, "Onset of Film Boiling", was selected to describe the two mechanisms. The authors' interpretation of the CHF mechanism is that it is governed by hydrodynamic instabilities and represents an instantaneous transition from nucleate to film boiling (DNB). The local dryout mechanism does not follow nucleate boiling, and represents an instantaneous transition from single-phase natural convection to film boiling upon boiling incipience. Each of the two mechanisms (local dryout and hydrodynamic CHF) result in film boiling, therefore we introduced the term "Onset of Film Boiling" (OFB), and will refer to it throughout the paper. Upcoming photographs

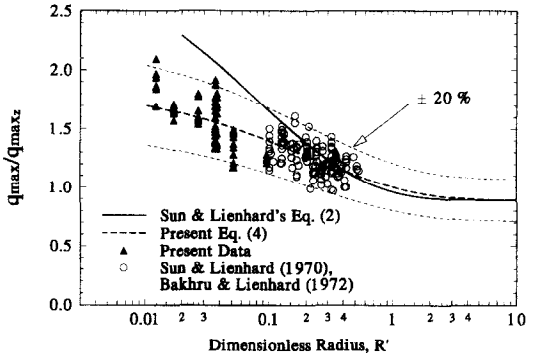

FIG. 3. q_{max} correlation for hydrodynamic CHF.

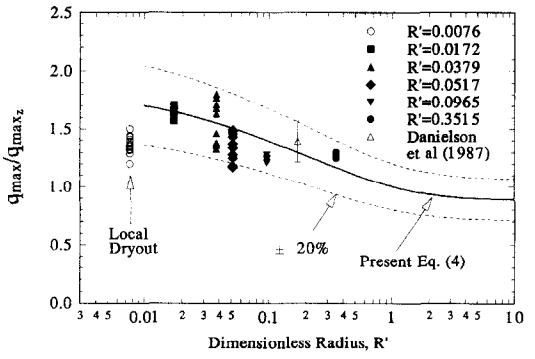

FIG. 4. q_{max} correlation; saturated FC-72.

will illustrate the differences between these two mechanisms.

Modified hydrodynamic CHF correlation

As previously pointed out by Bakhru and Lienhard [7], hydrodynamic instabilities determine the departure from nucleate boiling when R' is greater than 0.12–0.15. For these conditions, a fully developed nucleate boiling regime was observed prior to the CHF point. This is identified as the "hydrodynamic CHF" mechanism, as opposed to the "local dryout" mechanism. The present data exhibit hydrodynamic CHF mechanisms for R' values much lower than 0.12–0.15; see Table 1.

Based upon the current results representing all hydrodynamic CHF conditions (Table 1), the hydrodynamic CHF correlation, equations (2), developed by Sun and Lienhard [6] has been modified for smaller R' values ($R' < 0.0123$).

$$\frac{q_{max}}{q_{max_z}} \cong 0.89 + 1.01e^{-2.18\sqrt{R'}}; \quad R' > 0.0123. \quad (4)$$

Figure 3 illustrates Sun and Lienhard's correlation [6], equation (2), and the modified correlation, equation (4), with available hydrodynamic CHF data, including Sun and Lienhard [6] and Bakhru and Lienhard [7]. It is shown that the modified hydrodynamic CHF correlation begins to differ, predicts lower, and improves the prediction compared to the previous correlation at R' values less than 0.3. The modified prediction is accurate to within $\pm 20\%$ for $R' > 0.0123$.

FC-72 experiments

The dimensionless heat flux at the onset of film boiling is plotted against the dimensionless radius for saturated FC-72 conditions (Fig. 4). The data of Danielson *et al.* [9] compare well with the modified correlation at $R' \sim 0.2$. The current data (closed symbols) follow the characteristic hydrodynamic CHF mechanism for R' values ranging from 0.3515 down to 0.0172. At an R' value of 0.0076, the data deviate from the modified correlation, indicating the breakdown of the hydrodynamic CHF mechanism as will be evident in the upcoming discussion. The dimensionless radius (R') value for which the hydrodynamic mechanism disappears at saturated FC-72 conditions lies between 0.0172 and 0.0076.

Figure 5 illustrates saturated FC-72 boiling curves for two wire sizes, 11 and 75 μm, which lead to R' values of 0.0076 and 0.0517, respectively. The solid lines represent the natural convection correlation of Kuehn and Goldstein [10] for each wire size. Excellent agreement between the measured natural convection data and Kuehn and Goldstein's correlation is observed, lending confidence to the measurement accuracy. The trend of increasing heat transfer with decreasing wire size is observed in the natural convection region.

The most important observation in Fig. 5 is the absence of nucleate boiling on the 11 μm ($R' = 0.0076$) wire. As the heat flux is increased through the natural convection region, at some point vaporization (nucleation) occurs. At that instant, bubble growth occurs in both the radial and axial direction, after which, due to the ratio of the bubble departure diameter to the physical wire diameter, bubble growth and expansion is confined to the axial direction along the wire. This confined vapor expansion causes the wire temperature to increase and in turn, instantaneous vaporization of adjacent superheated liquid in contact with the wire. This mechanism is referred to as "local dryout". As illustrated in Fig.

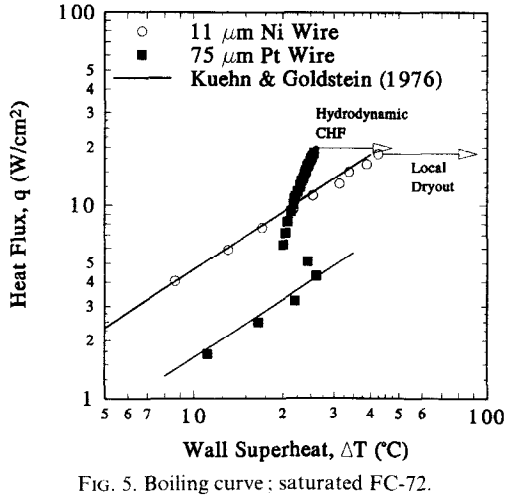

FIG. 5. Boiling curve; saturated FC-72.

5, at the end of the natural convection region, the wire temperature increases significantly (~50°C) indicating the local dryout mechanism. Figure 6 shows three consecutive photographs which illustrate the local dryout mechanism encountered on the 11 μm diameter wire during 0.067 s. Figure 6(a) shows a condition just prior to local dryout (time = 33:29) where no bubbles have formed on the wire (note the 11 μm wire is not visible). The small bubble leaving the right copper terminal is caused by the solder joint at the wire–terminal junction and does not reflect nucleation from the wire. Figure 6(b) illustrates the local dryout mechanism, 0.033 s after the natural convection condition shown in Fig. 6(a). Within 1/30th of a second, single-phase natural convection ceases, nucleation is initiated, and bubble growth is confined to the wire axis as is observed in Fig. 6(b). From the figure, the propagation velocity at which the vapor–liquid interface travels along the wire was calculated to be greater than 0.1 m s^{-1}. This axial bubble growth results in a vapor blanket covering the wire and an instantaneous increase in wire temperature. It should be noted that nucleate boiling was never established. Figure 6(c) represents a condition 1/30th of a second after local dryout occurrence (Fig. 6(b)). The wire temperature increase (~50°C) was sensed and electrical power to the wire was terminated.

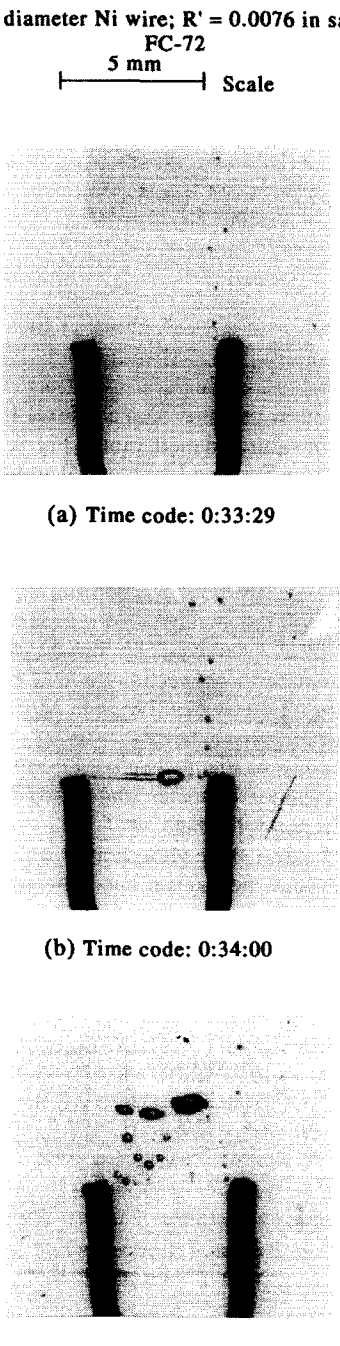

(a) Time code: 0:33:29

(b) Time code: 0:34:00

(c) Time code: 0:34:01

FIG. 6. Local dryout mechanism.

Data representative of the 75 μm wire (Fig. 5) clearly indicate fully developed nucleate boiling between 6 and 19 W cm^{-2}. For these conditions, upon the occurrence of boiling incipience, the bubble growth and expansion is not confined to the axial wire direction due to the decreased ratio of the bubble departure to wire diameters. Fully developed nucleate boiling occurs and the OFB is governed by hydrodynamic instabilities. Figure 7 shows a photograph which illustrates the hydrodynamic CHF mechanism encountered on the 75 μm diameter wire. The hydrodynamic CHF mechanism is a transient phenomenon where transition from nucleate to film boiling occurs. The figure clearly indicates both film and nucleate boiling phenomena. The right 30% of the wire is observed to be covered with smaller bubbles (nucleate boiling) having departure diameters between ~ 0.6 and 1.0 mm. This is in good agreement with the Cole and Rohsenow [11] correlation for FC-72 (~0.8 mm). The left portion of the wire (~70%) is seen to be covered by a vapor blanket, the base of the bubbles being fed by the film and observed to be significantly wider than those over the nucleate boiling region. The wavelength over this portion of the wire is observed to be ~1.2 mm, ~15% of the Taylor one-dimensional wavelength (~8 mm) for FC-72. Observations from the largest wire tested in FC-72 (R' = 0.3515) indicated a departing wavelength of 4 mm, ~50% of the Taylor one-dimensional wavelength (not shown here). These differences can be attributed to the small wire diameter, with the difference decreasing as the wire diameter increases.

R-113 *experiments*

Another highly-wetting liquid (R-113) having a low surface tension is used for testing. Dimensionless heat flux data at the OFB is plotted against the dimensionless radius for saturated conditions in Fig. 8. R-113 data from Elkassabgi and Lienhard [12] is shown for R' values greater than 0.1 and compares well with the current hydrodynamic CHF correlation. The current data follow the trend of hydrodynamic CHF for R' values from 0.0369 down to 0.0123. For these R'

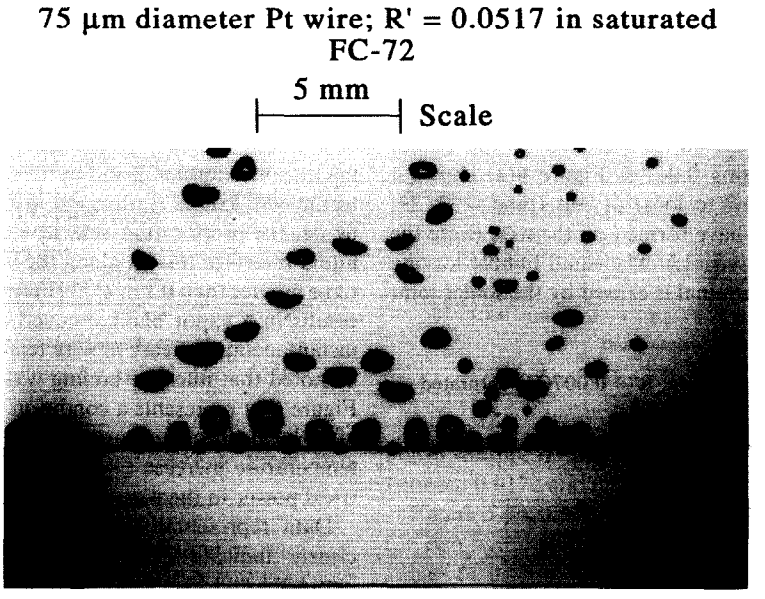

FIG. 7. Hydrodynamic CHF mechanism.

values, fully developed nucleate boiling was observed prior to the maximum heat flux (hydrodynamic CHF) occurrence. At an R' value of 0.0054, the data deviate from the modified correlation, indicating the breakdown of the hydrodynamic CHF mechanism. For this condition, the local dryout mechanism previously discussed (Figs. 4–6) governs the OFB condition, showing consistency with FC-72. The dimensionless radius (R') value for which the hydrodynamic mechanism disappears at saturated R-113 conditions lies between 0.0123 and 0.0054. Photographs and boiling data for R-113 did not show any differences in the trends observed using FC-72.

Methanol experiments

Methanol is a non-highly-wetting liquid in comparison to FC-72 and R-113. Its increased surface tension produces stronger bonding forces than that of the highly-wetting liquids and results in larger (~100%) bubble departure diameters during nucleation. When the bubble departure diameter increases, larger physical wire diameters are required to prevent local dryout mechanism occurrence. It is expected that wire sizes resulting in hydrodynamic CHF mechanisms in highly-wetting liquids could produce the local dryout mechanism for methanol.

Dimensionless heat flux data at the OFB is plotted against R' for saturated methanol in Fig. 9. Methanol data taken from Sun and Lienhard [6] and Elkassabgi and Lienhard [12] for R' values larger than 0.1 compare well with the modified hydrodynamic CHF correlation. As expected, the current data indicate occurrence of the local dryout mechanism, and no fully-developed nucleate boiling or hydrodynamic CHF mechanism was observed. An instantaneous transition from natural convection to film boiling was observed for all four wires. Ivey and Morris [13] and Gaidarov *et al.* [14] observed the similar trend of q_{max} variation shown in Fig. 9. The fall-off in CHF below a certain cylinder diameter and sharp increase as diameter decreases further.

Figure 10 shows three photographs which illustrate the local dryout mechanism encountered on the 25 μm diameter wire in the non-highly-wetting liquid, methanol. Figure 10(a) shows a condition just prior to local dryout where no bubbles have formed. Figure

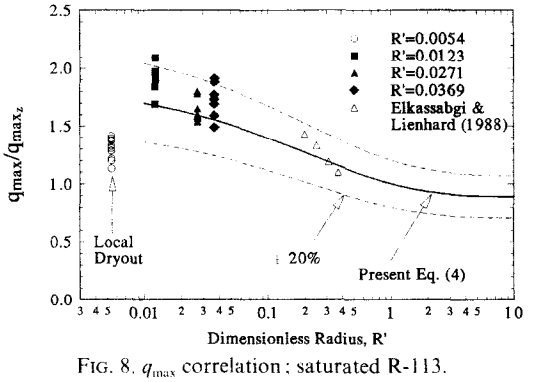

FIG. 8. q_{max} correlation; saturated R-113.

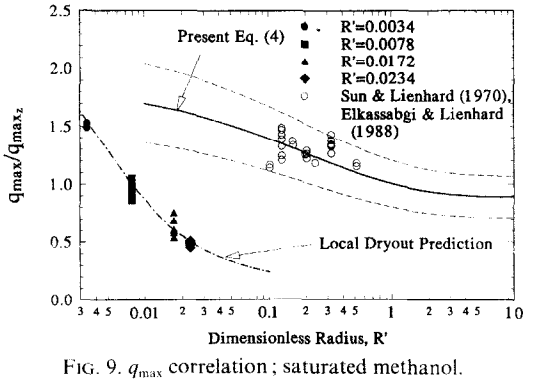

FIG. 9. q_{max} correlation; saturated methanol.

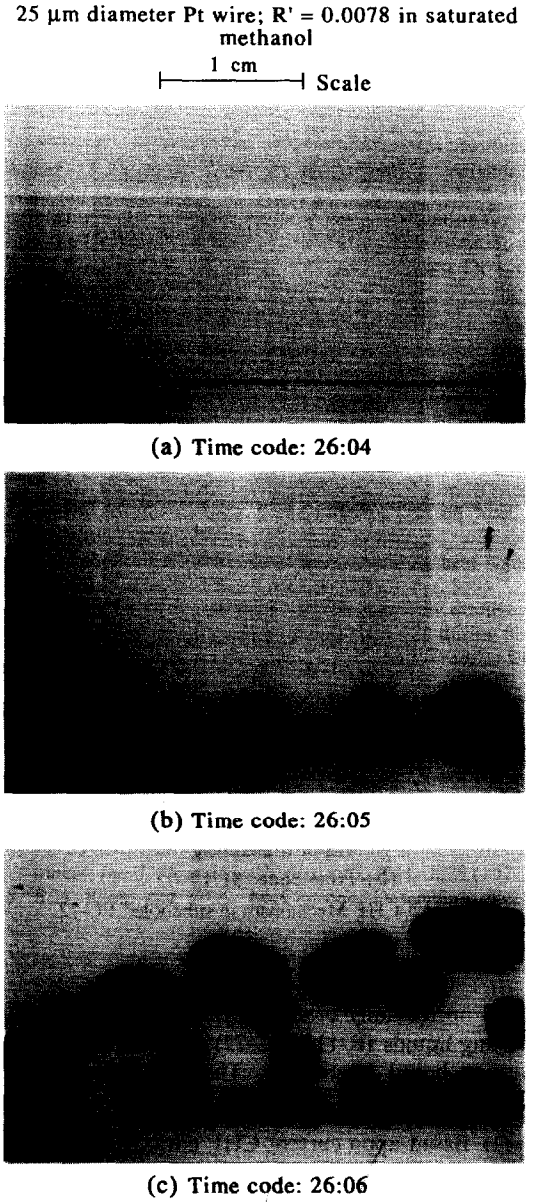

FIG. 10. Local dryout mechanism.

10(b) illustrates the local dryout mechanism, 0.033 s after Fig. 10(a). During that 1/30th of a second, nucleation is initiated and bubbles grow and merge together on the wire surface. This merging of bubbles is indicated by the size of the bubbles in Fig. 10(b), ~3–6 mm, which are larger than the departure diameter for methanol as predicted by the Cole and Rohsenow [11] correlation, ~1.7 mm. This local dryout mechanism is similar to that reported by Bakhru and Lienhard [7] but it appears to be different from that of the highly-wetting liquids. Figure 6 showed the bubble growth in FC-72 was confined to axial direction resulting in vapor blanketing. For methanol test conditions (Fig. 10), 2–4 neighboring bubbles agglomerate together and form a vapor blanket over significant portions of the wire, resulting in a large temperature increase. When a temperature increase greater than 20°C is sensed, electrical power is terminated and smaller bubbles are observed on the wire (Fig. 10(c)).

The local dryout mechanism shown in Fig. 10 is observed for all four methanol test conditions. This mechanism is the result of an instantaneous transition from single-phase natural convection to film boiling upon the beginning of nucleation as discussed by Bakhru and Lienhard [7] and Hong *et al.* [15]. Because the local dryout condition occurs at the onset of nucleation, this mechanism is governed by boiling incipience. Griffith and Wallis [16] suggested an expression for predicting the wall superheat, ΔT, at the boiling incipience point.

$$\Delta T = T_w - T_{sat}(P_l) \approx \frac{2\sigma T_{sat} v_{fg}}{h_{fg} r_c}, \quad (5)$$

where r_c is the cavity radius. Bar-Cohen and Simon [17] revised this expression,

$$\Delta T = T_w - T_{sat}(P_l) \approx T_{sat}(P_l + 2\sigma(T_w)/r_b) - T_{sat}(P_l) \quad (6)$$

where r_b is the radius of the embryonic bubble within the surface cavities. For the four cases, the departure from natural convection (DNC) and local dryout point coincide. Therefore, the local dryout heat flux value can be predicted for a known embryonic bubble size. Using the observed methanol incipience superheat (~70°C) in equation (6), an embryonic bubble size was calculated (~0.028 μm). Based on the ratio of the embryonic bubble size to the wire diameters investigated (11–510 μm, Table 1), an assumption was made that each wire has a statistically consistent surface micro-geometry regardless of its diameter, therefore, incipience is assumed to occur for all wires at the indicated superheat. The natural convection heat flux at this superheat (~70°C) was then calculated using the single-phase natural convection correlation of Kuehn and Goldstein [10] for varying wire diameters. For natural convection, smaller wire diameters provide more efficient heat transfer. The current data (Fig. 9) show excellent agreement with the local dryout prediction using boiling incipience theory.

Further discussions concerning onset of film boiling in subcooled FC-72

From the data shown for FC-72 (Fig. 4), R-113 (Fig. 8), and methanol (Fig. 9), the transition where the hydrodynamic CHF mechanisms cease and the local dryout mechanisms become dominant is observed as wire size decreases. Hong *et al.* [15] developed a correlation to predict the transition R' value by relating wire diameter to bubble departure at which the hydrodynamic mechanisms cease. For saturated FC-72 conditions, the 11 μm wire ($R' = 0.0076$) did not generate any nucleate boiling, the OFB being governed by the local dryout mechanism. As previously discussed and observed in

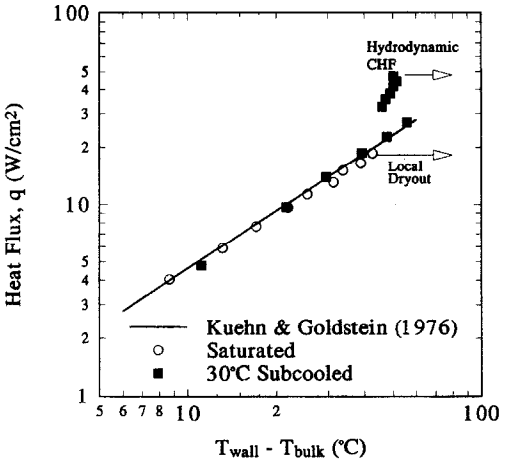

FIG. 11. Boiling curve of 11 μm dia. wire in saturated and subcooled FC-72.

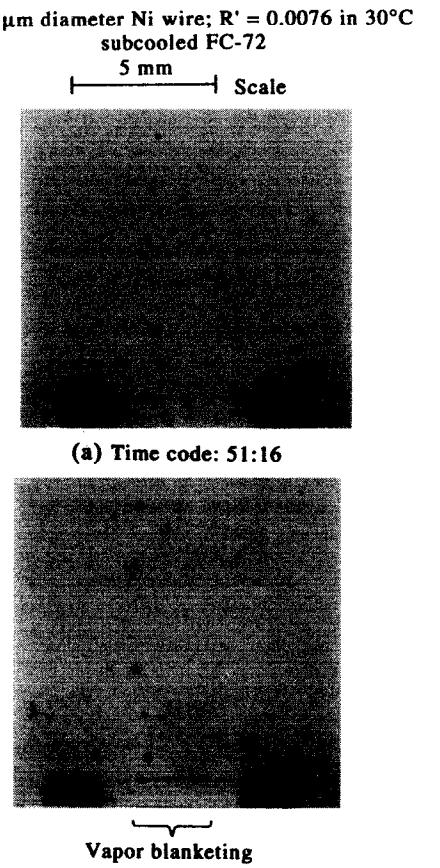

FIG. 12. CHF Mechanism in subcooled FC-72.

Fig. 6, the local dryout mechanism occurs just after incipience.

Data measured from the same wire (11 μm) in 30°C subcooled FC-72 are shown in Fig. 11. For this condition, nucleate boiling is observed, preventing local dryout at incipience. This is caused by subcooled bulk liquid around the wire at the onset of nucleation. Under saturated conditions, once nucleation of the bubble begins, it occurs spontaneously. During this vaporization process, the bubble is constrained to growth along the wire axis, resulting in local film boiling. Under subcooled conditions, the bubble is exposed to "cooler" bulk liquid. This cooler bulk liquid condenses the vapor inside the bubble, decreasing the bubble size and preventing it from spontaneous growth along the wire axis. As a result in the subcooled case, boiling incipience is completed, and fully developed nucleate boiling is achieved (Fig. 11). Figure 12 illustrates two successive photographs taken from the 11 μm wire in FC-72 at 30°C of subcooling. In Fig. 12(a), nucleate boiling is observed just prior to the CHF occurrence. The departure diameter of the bubbles at this condition is ~0.3 mm, ~50% smaller than that in saturated FC-72 (0.6–1.0 mm as discussed with Fig. 7). Figure 12(b) shows the OFB phenomena on the wire 0.033 s after the nucleate boiling condition illustrated in Fig 12(a). Although the resolution does not allow the detection of the instability mechanisms which govern the hydrodynamic CHF, it is proposed that due to the subcooled bulk fluid, a vapor blanket exists over ~50% of the wire length. This subcooling effect, which has changed the CHF mechanism from dryout to hydrodynamic situation, agrees with the observation of Kutateladze *et al.* [18].

CONCLUSIONS

Pool boiling experiments are performed to investigate the onset of film boiling (OFB) mechanisms on small horizontally oriented cylinders in two highly-wetting liquids (R-113, FC-72) and one non-highly-wetting liquid (methanol). The conclusions are as follows:

(1) Based upon current CHF data, Sun and Lienhard's [6] CHF correlation was modified. The modified correlation, which is valid for the hydrodynamic CHF mechanism, shows improved prediction capability for smaller R' values ($R' < 0.3$).

(2) Two different onset of film boiling mechanisms, hydrodynamic CHF and local dryout were identified. The hydrodynamic mechanism accompanies nucleate boiling. The local dryout mechanism is present upon boiling incipience.

(3) The local dryout mechanism for highly-wetting liquids is governed by an axial bubble growth pattern. Its existence is dependent upon the ratio of the bubble departure to wire diameter. The local dryout mechanism for non-highly-wetting liquids is governed by bubble growth and coalescence on the wire.

(4) A method of predicting the local dryout mechanism was suggested using boiling incipience theory and the natural convection correlation of Kuehn and Goldstein [10]. The prediction showed excellent agreement with experimental data.

(5) Subcooling eliminates the occurrence of local

dryout mechanism by generating a fully developed nucleate boiling regime due to condensation of the bubble.

Acknowledgements—This study was supported by the Texas Higher Education Coordinating Board: Advanced Research/Technology Program Grant number 003656-101. Support was also provided by the Research Initiation Grant from the University of Texas at Arlington. The donation of FC-72 from the 3M Industrial Chemical Products Division is appreciated.

REFERENCES

1. S. Nukiyama, The maximum and minimum values of the heat Q transmitted from metal to boiling water under atmospheric pressure, *Int. J. Heat Mass Transfer* **9**, 1419–1433 (1934) (translated in 1966).
2. S. S. Kutateladze, Teploperedacha pri kondensatsii kipenii, State Sci. and Tech. Pubs of Lit. on Mach., Moscow (1952).
3. N. Zuber, Hydrodynamic aspects of boiling heat transfer, Ph.D. Thesis, UCLA, Los Angeles, CA (1959).
4. J. H. Lienhard and P. T. Y. Wong, The dominant unstable wavelength and minimum heat flux during film boiling on a horizontal cylinder, *J. Heat Transfer* **86**, 220–226 (1964).
5. J. H. Lienhard and K. Watanabe, On correlating the peak and minimum boiling heat fluxes with pressure and heater configuration, *J. Heat Transfer* **88**, 94–100 (1966).
6. K. H. Sun and J. H. Lienhard, The peak pool boiling heat flux on horizontal cylinders, *Int. J. Heat Mass Transfer* **13**, 1425–1439 (1970).
7. N. Bakhru and J. H. Lienhard, Boiling from small cylinders, *Int. J. Heat Mass Transfer* **15**, 2011–2025 (1972).
8. S. J. Kline and F. A. McClintock, Describing uncertainties in single-sample experiments, *Mech. Engng* **75**, 3–8 (1953).
9. R. D. Danielson, L. Tousignant and A. Bar-Cohen, Saturated pool boiling characteristics of commercially available perfluorinated inert liquid, *Proceedings of ASME/JSME Thermal Engineering Joint Conference*, Vol. 3, pp. 419–430 (1987).
10. T. H. Kuehn and R. J. Goldstein, Correlating equations for natural convection heat transfer between horizontal circular cylinders, *Int. J. Heat Mass Transfer* **19**, 1127–1134 (1976).
11. R. Cole and W. M. Rohsenow, Correlation of bubble departure diameter for boiling of saturated liquids, Chem. *Engng Prog. Symp. Ser.* **65**, 211–213 (1969).
12. Y. Elkassabgi and J. H. Lienhard, Influence of subcooling on burnout of horizontal cylindrical heaters, *J. Heat Transfer* **110**, 479–486 (1988).
13. H. J. Ivey and D. J. Morris, The effect of test section parameter on saturation pool boiling burnout at atmospheric pressure, *Chem. Engng Prog. Symp. Ser.* **61**(60), 157–166 (1965).
14. Sh. A. Gaidarov, L. N. Grigor'ev and A. G. Usmanov, Effect of heater diameter on critical heat flux in boiling, *J. Appl. Mech. Tech. Phys.* **3**, 99 (1965).
15. Y. S. Hong, S. M. You and J. P. O'Connor, Critical heat flux mechanism on small cylinders, *Proceedings of 6th International Symposium on Transport Phenomena in Thermal Engineering*, Seoul, Korea (1993).
16. P. Griffith and J. D. Wallis, The role of surface conditions in nucleate boiling, *Chem. Engng Prog. Symp. Ser.* **56**, 49–63 (1959).
17. A. Bar-Cohen and T. W. Simon, 1988, Wall superheat excursions in the boiling incipience of dielectric fluids, *Heat Transfer Engng* **9**, 19–31 (1988).
18. S. S. Kutateladze, N. V. Volukina and I. I. Gogonin, Effects of heater size on critical heat loads in the boiling of a liquid with free convection, *Teplofzika Vysokikh Temperatur* **5**(5), 841 (1967).